

Astrocytes increase the activity of synaptic GluN2B NMDA receptors

Junghyun Hahn, Xianhong Wang and Marta Margeta*

Department of Pathology, University of California San Francisco, San Francisco, CA, USA

Astrocytes regulate excitatory synapse formation and surface expression of glutamate AMPA receptors (AMPA) during development. Less is known about glial modulation of glutamate NMDA receptors (NMDARs), which mediate synaptic plasticity and regulate neuronal survival in a subunit- and subcellular localization-dependent manner. Using primary hippocampal cultures with mature synapses, we found that the density of NMDA-evoked whole-cell currents was approximately twice as large in neurons cultured in the presence of glia compared to neurons cultured alone. The glial effect was mediated by (an) astrocyte-secreted soluble factor(s), was Mg^{2+} and voltage independent, and could not be explained by a significant change in the synaptic density. Instead, we found that the peak amplitudes of total and NMDAR miniature excitatory postsynaptic currents (mEPSCs), but not AMPAR mEPSCs, were significantly larger in mixed than neuronal cultures, resulting in a decreased synaptic AMPAR/NMDAR ratio. Astrocytic modulation was restricted to synaptic NMDARs that contain the GluN2B subunit, did not involve an increase in the cell surface expression of NMDAR subunits, and was mediated by protein kinase C (PKC). Taken together, our findings indicate that astrocyte-secreted soluble factor(s) can fine-tune synaptic NMDAR activity through the PKC-mediated regulation of GluN2B NMDAR channels already localized at postsynaptic sites, presumably on a rapid time scale. Given that physiologic activation of synaptic NMDARs is neuroprotective and that an increase in the synaptic GluN2B current is associated with improved learning and memory, the astrocyte-induced potentiation of synaptic GluN2B receptor activity is likely to enhance cognitive function while simultaneously strengthening neuroprotective signaling pathways.

Keywords: NMDA receptor, GluN2B subunit, astrocytes, synapses, protein kinase C

Introduction

Glial cells play a critical role in the formation and function of excitatory synapses. In particular, it is well established that during development astrocyte-secreted soluble messengers promote synapse formation and surface expression of glutamate AMPA receptors (AMPA) in both retinal ganglion cells and hippocampal neurons (Ullian et al., 2001; Christopherson et al., 2005; Xu et al., 2010; Allen et al., 2012). Much less is known about glial regulation of NMDA glutamate receptors (NMDARs), which together with AMPARs mediate excitatory postsynaptic signaling.

NMDARs are crucial for a wide range of brain functions, including synaptic plasticity and neural development (Cull-Candy and Leszkiewicz, 2004; Zito et al., 2009). NMDAR dysfunction

OPEN ACCESS

Edited by:

Vladimir Parpura,
University of Alabama, USA

Reviewed by:

Rheinallt Parri,
Aston University, UK
Takumi Takizawa,
Gunma University, Japan

*Correspondence:

Marta Margeta,
Department of Pathology, University
of California San Francisco, UCSF
Pathology, Box 0511, 513 Parnassus
Ave., HSW-514, San Francisco, CA
94143, USA
Tel: 415-514-0228,
Fax: 415-514-3165
Marta.Margeta@ucsf.edu

Received: 13 January 2015

Accepted: 15 March 2015

Published: 17 April 2015

Citation:

Hahn J, Wang X and Margeta M
(2015) Astrocytes increase the
activity of synaptic GluN2B NMDA
receptors.
Front. Cell. Neurosci. 9:117.
doi: 10.3389/fncel.2015.00117

is implicated in many neurologic and psychiatric disorders (Cull-Candy et al., 2001; Hardingham and Bading, 2003; Schwartz et al., 2012), highlighting the importance of the precise regulation of NMDAR activity. NMDAR functional diversity is controlled through two distinct mechanisms: subunit composition and subcellular localization (Paoletti et al., 2013; Sanz-Clemente et al., 2013). NMDAR channels consist of two GluN1 and two GluN2 subunits, with GluN2 subunits conferring distinct functional properties on the assembled heterotetrameric channel complexes. Hippocampal neurons primarily express GluN1/GluN2A and GluN1/GluN2B NMDARs; in comparison with GluN1/GluN2A channels, GluN1/GluN2B channels have higher glutamate and glycine sensitivity, lower open probability, and slower deactivation kinetics (Paoletti et al., 2013). In addition, GluN2A and GluN2B subunits differ in their binding affinities for various intracellular scaffolding and signaling proteins (Paoletti et al., 2013). Irrespectively of the subunit composition, NMDAR coupling to intracellular signaling cascades also depends on the receptor subcellular localization. Although non-physiologic (tonic) activation of synaptic NMDARs can lead to excitotoxicity (Parsons and Raymond, 2014), these receptors preferentially couple to neuroprotective signaling pathways when activated by physiologic (phasic) stimuli (Hardingham and Bading, 2010; Martel et al., 2012). In contrast, activation of extrasynaptic NMDARs is generally neurotoxic and has been implicated in the pathogenesis of several neurodegenerative disorders (Parsons and Raymond, 2014).

Astrocytes can activate NMDARs by secreting the NMDAR ligands glutamate and D-serine, thus directly modulating synaptic efficacy and plasticity (Haydon and Carmignoto, 2006; Lee et al., 2007; Perea and Araque, 2010; Han et al., 2013). Astrocytes were also shown to regulate the surface expression of GluN2A and GluN2B NMDARs (Fellin et al., 2009; Deng et al., 2011), but a recent study raised the possibility that these findings were an artifact of the transgenic model system used for experiments (Fujita et al., 2014). Here, we use wild-type hippocampal cultures with mature synapses to show that astrocytes secrete a soluble factor or factors that increase the activity, but not the cell surface expression, of synaptic GluN2B-containing NMDARs through a protein kinase C (PKC)-mediated mechanism. Thus, astrocytes can regulate NMDAR function in both a subunit- and localization-specific manner, without altering the trafficking of NMDAR channel subunits.

Materials and Methods

Cell Cultures

Mixed, neuronal, and astrocytic primary hippocampal cultures were prepared from E18–E19 embryos obtained from Sprague-Dawley rats (Charles River), as described previously (Habas et al., 2013). All procedures involving animals were approved by the UCSF Animal Care and Use Committee. Mixed cell suspension was plated at a density of 600 cells/mm², either in tissue culture dishes coated with 0.1 mg/mL poly-L-lysine or on 12-mm glass cover slips (Bellco) coated with the mixture of

poly-L-lysine and laminin. To obtain predominantly neuronal cultures, a subset of cultures was treated with 1 μM AraC (Sigma) to suppress glial cell growth; mixed cultures were left untreated. Mixed and neuronal cultures were grown in Neurobasal/B27 culture medium for 2–3 weeks before experiments. For astrocytic cultures, hippocampal cell suspension was plated in 75 cm² tissue culture flasks and grown in DMEM/fetal bovine serum culture medium. One week after plating (when the astrocyte layer became confluent), cultures were vigorously shaken (300 rpm at 37°C) overnight to remove microglia and oligodendroglia; astrocytes were then trypsinized, re-plated into 175 cm² tissue culture flasks, and maintained for another 3–4 days before being used for direct or indirect neuron-astrocyte co-cultures (Habas et al., 2013). For direct co-cultures, astrocytes were plated into DIV10 AraC-treated neuronal cultures at a density of ~120 cells/mm²; for indirect co-cultures, astrocytes were plated at the same density on cell culture inserts, which were then placed on top of DIV10 neuronal cultures. (The insert membrane has a pore size of 1 μm and is separated from the well bottom by 800 μm; this culture arrangement allows neurons and astrocytes to exchange soluble factors while preventing a direct cell-cell contact.). In both co-culture arrangements, the two cell types were cultured together for 4–7 days prior to experiments.

Electrophysiology

DIV13–17 neurons were used for patch-clamp recordings. NMDA-evoked currents were recorded at –60 mV (except in I/V analysis experiments) in the external solution containing (in mM) 135 NaCl, 5 KCl, 2 CaCl₂, 1.2 MgCl₂, 10 HEPES, and 10 glucose, with 1 μM glycine, 10 μM bicuculline, and 1 μM TTX (~305 mOsm, pH 7.4); for 0 Mg²⁺ external solution, MgCl₂ was replaced with glucose. The pipette solution contained (in mM) 120 CsCl, 20 TEA-Cl, 1 MgCl₂, 1 CaCl₂, 2.25 EGTA, 10 HEPES, 2.5 Mg₂ATP, 1 Na₃GTP (~298 mOsm, pH 7.4; calculated free Ca²⁺ concentration, 70 nM). The liquid junction potential, measured with 3 M KCl, was –8.8 mV and was not adjusted except for I/V and unitary conductance analyses. mEPSC recording solutions were adapted from previously published studies (Watt et al., 2000; Fu et al., 2005; Lee et al., 2007). For total excitatory mEPSC recordings, 0 Mg²⁺ external solution was supplemented with 10 μM glycine, 1 μM TTX, and 20 μM bicuculline; AP5 (100 μM) was added to isolate AMPAR-mediated mEPSCs, while 1 μM strychnine and 10 μM NBQX were added to isolate NMDAR-mediated mEPSCs. The pipette solution contained (in mM): 125 K-gluconate, 10 KCl, 10 Na-phosphocreatine, 2.25 EGTA, 2.5 Mg₂ATP, 0.5 Na₃GTP, 10 HEPES (~297 mOsm, pH 7.4); this pipette solution was also used for whole-cell recordings in MK-801 experiments. Drugs were purchased from Tocris Bioscience [except for bicuculline (Sigma-Aldrich) and thrombospondin (Haematologic Technologies)] and were applied through an electronically controlled, gravity-fed perfusion system with a response time of 15–20 ms (ALA Scientific); after placing a cell in the center of the visual field under 10× objective, the perfusion tip with an opening diameter of 500 μm was placed at the field edge. The pipette electrodes were pulled

from borosilicate glass tubes (Sutter Instruments) and had resistances of 3.5–4.2 M Ω . Recordings were obtained using a Multiclamp 700B amplifier (Molecular Devices), with signals filtered at 1 kHz and sampled at 10 kHz using a Digidata 1440A analog-to-digital converter (Molecular Devices). All data were recorded and analyzed with pClamp 10 software (Molecular Devices).

mEPSC Analysis

mEPSC data were analyzed using the Mini Analysis Program (Synaptosoft). Total and AMPAR mEPSC amplitudes were calculated by averaging the peak amplitudes of all individual mEPSC events recorded from a single neuron in the absence (total mEPSCs) or presence of AP5 (AMPAR mEPSCs). To obtain the average NMDAR-mediated mEPSC amplitude from the same set of recordings, the average AMPAR mEPSC trace (obtained by aligning and averaging all mEPSC events recorded from one neuron in the presence of AP5) was subtracted from the average total mEPSC trace (obtained by aligning and averaging all events recorded from the same neuron in the absence of AP5). In a separate set of recordings, NMDAR mEPSCs were recorded directly after blocking AMPAR mEPSCs with NBQX; for these experiments, NMDAR mEPSC amplitude was calculated by averaging the peak amplitudes of all individual NMDAR mEPSCs (amplitude threshold, 7 pA) recorded from a single neuron. To perform kinetic separation of AMPAR and NMDAR mEPSC components, we followed the general procedure described by Watt et al. (2000), except that the specific time points used for measurement of AMPAR and NMDAR mEPSC components were determined based on pharmacologic experiments performed in our cultures. Specifically, AMPA mEPSCs recorded in the presence of AP5 peaked close to 1 ms in both neuronal and mixed cultures, while NMDA mEPSCs recorded in the presence of NBQX, bicuculline, and strychnine peaked at 7.2 ± 0.6 ms in neuronal cultures and at 14.2 ± 1.0 ms in mixed cultures ($n = 50$ – 60). The residual AMPA mEPSCs were less than 1 pA when measured 7 ms after the peak in neuronal cultures or 15 ms after the peak in mixed cultures, indicating that total mEPSCs were not contaminated by AMPAR components around those time points. For kinetic analysis of the NMDAR/AMPA ratio, we therefore measured the NMDA mEPSC peak (averaged over 1 ms) from total mEPSCs in a window of 6–10 ms after the AMPA mEPSC peak in neuronal cultures and in a window of 13–17 ms after the AMPA mEPSC peak in mixed cultures. To exclude synapses containing only AMPA components, we selected mEPSC events in which the NMDA mEPSC peak was larger than 2 pA.

Immunofluorescence

Cells were fixed for 30 min on ice in 4% paraformaldehyde in PBS, washed three times in ice-cold PBS, and blocked for 30 min in a blocking buffer (2% goat serum and 0.25% Triton X-100 in PBS). Cells were then incubated overnight at 4°C with primary antibodies [guinea pig polyclonal anti-synaptophysin (Synaptic System, 1:1000) and mouse

monoclonal anti-PSD-95 (6G6-1C9, Abcam, 1:300)], washed three times with PBS at room temperature (RT), and then incubated for an hour at RT with secondary antibodies [Alexa-594-conjugated goat anti-guinea pig (Molecular Probes, 1:1000) and Alexa-488-conjugated goat anti-mouse (Molecular Probes, 1:1000)]. Following 5 min RT incubation with DAPI nuclear dye, coverslips were washed three times in PBS and mounted in Fluoromount-G (Cell Lab, Beckman Coulter).

Imaging

Images were acquired with a spinning disk confocal microscope (Yokogawa). A healthy-appearing neuron that was about two cell diameters away from its neighbors was placed in the center of the camera field to capture digital images of fluorescence emissions at 488 nm and 594 nm using MetaMorph image capture software. The selected cell was imaged in serial optical sections at 0.33 μ m intervals over a total depth of 5 μ m, for a total of 15 optical sections. Maximum intensity projections (MIPs) were generated from these sections, yielding 5 MIPs representing 1 μ m of depth each; fluorescence intensity in each MIP was quantified as described previously (Ippolito and Eroglu, 2010). Synaptic puncta, defined by co-localization of synaptophysin and PSD-95 labeling, were quantified in the selected regions of interest (ROI; $89 \times 89 \mu$ m square) using Puncta Analyzer program written by Bary Wark for ImageJ 1.26.¹ A total of 9 cells from 3 coverslips (each coverslip from a different culture batch) were analyzed for each experimental condition.

Western Blotting

Cells were lysed on ice with modified RIPA buffer (0.5% SOD, 0.1% SDS, 1% Triton X-100, 150 mM NaCl, 50 mM TrisCl, 1 mM EDTA) supplemented with a protease inhibitor cocktail (Roche). Crude lysates were cleared by centrifugation at 6000 rpm for 10 min at 4°C, solubilized with LDS sample buffer (Invitrogen) supplemented with TCEP reducing reagent (Pierce; final concentration 12.5 mM), and heated for 10 min at 70°C prior to loading; given different cellular compositions of the cultures, samples were loaded on an equal volume basis. Samples were electrophoretically resolved with 4–12% Bis-Tris NuPAGE gels (Invitrogen) and electroblotted to nitrocellulose membranes. Membranes were blocked for 1 h at RT in TBS (150 mM NaCl, 20 mM TrisCl; pH = 7.4) containing 3% nonfat dried milk, incubated with primary antibodies for 2–3 h at RT or overnight at 4°C, washed 4 times at RT, incubated with the corresponding secondary antibody for 1 h at RT, and washed for at least 30 min at RT. Following a final wash in TBS with 0.1% Tween for 10 min at RT, protein-antibody complexes were detected using an ECL chemiluminescent kit (Pierce Biotechnology) and CL-XPosure Film (Thermo Scientific) with a Konica SRX-101A film developer. In a subset of experiments (Figure 10), the Odyssey Fc infrared imaging system (LI-COR Biosciences) was used for detection of the protein-antibody complexes. In these experiments, electrophoresis was performed using 3–8%

¹<http://rsbweb.nih.gov/ij/>

Tris-Acetate NuPAGE gels (Invitrogen). The membranes were dried at RT for at least 1 h and then blocked with Odyssey Blocking Buffer (LI-COR Biosciences) for 1 h at RT. Odyssey Blocking Buffer supplemented with 0.1% Tween 20 was used for dilution of primary and secondary antibodies, while PBS supplemented with 0.1% Tween 20 was used for washing. Membranes were incubated with primary antibodies for 2 h at RT or overnight at 4°C, washed 4 times (5 min/wash) at RT, incubated with secondary antibodies for 1 h at RT, washed 4 times (5 min/wash) at RT, and then imaged using Odyssey Fc (LI-COR Biosciences) at 700 nm and 800 nm; images were analyzed using Image Studio Imaging Software (LI-COR Biosciences). Primary antibodies included: mouse monoclonal anti-NR1 (BD Biosciences, 1:1000), rabbit monoclonal anti-GluN2A (Millipore, 1:1000), mouse monoclonal anti-GluN2B (BD Biosciences, 1:100 [film] or 1:500 [Odyssey Fc]), rabbit polyclonal anti-phospho-GluN2B (Ser1303) (Millipore, 1:1000), mouse monoclonal anti-GluR1-NT (Millipore, 1:500), mouse monoclonal anti-PSD-95 (NeuroMab, 1:1000), rabbit polyclonal anti-synaptophysin (Santa Cruz Biotechnology, 1:1000) and mouse monoclonal anti-actin (Sigma, 1:5000). Secondary antibodies included goat horseradish peroxidase (HRP)-conjugated anti-rabbit secondary H + L IgG antibody and goat HRP-conjugated anti-mouse secondary H + L IgG antibody (Jackson ImmunoResearch, 1:5000 for both) or goat IRDye® 800CW-conjugated anti-rabbit secondary H + L IgG antibody and goat IRDye® 680RD-conjugated anti-mouse secondary H + L IgG antibody (LI-COR Biosciences, 1:15000 for both).

Surface Protein Biotinylation

After 2 washes with ice-cold PBS, live cultures were incubated with 1 mg/mL sulfo-NHS-S-S-Biotin (Pierce) for 20 min on ice. Following 2 washes with ice-cold PBS and 2 washes with ice-cold TBS (to remove and quench unbound reagent, respectively), cells were lysed in a modified RIPA buffer. Crude lysates were cleared by centrifugation at 6000 rpm for 10 min at 4°C; 10% of cleared lysate was reserved, while the rest was incubated with 50% NeutraAvidin agarose beads (Pierce) for 2–3 h or overnight at 4°C. After 5 washes with RIPA buffer, bound proteins were eluted with DTT- and TCEP-containing LDS sample buffer by heating for 30 min at 75°C; cleared whole cell lysate (input) and biotinylated protein fractions were then analyzed by Western blotting, as described above.

Data Fitting and Statistical Methods

Using a nonlinear least-squares algorithm, the dose-response data were fitted to Eq. 1 (where *Top* and *Bottom* are maximal and minimal current density values respectively, *y* is the current density obtained in response to a concentration of NMDA *x*, and *EC*₅₀ is the concentration of NMDA that yields the half-maximal current density).

$$y = \text{Bottom} + \frac{\text{Top} - \text{Bottom}}{1 + 10^{\text{LogEC}_{50} - x}} \quad (1)$$

The standard slope (Hill slope = 1) was adopted because (i) estimated Hill coefficients obtained from all groups were similar to 1 [0.9–1.4, as reported previously (Verdoorn and

Dingledine, 1988; Patneau and Mayer, 1990; Linsenbardt et al., 2013)]; and (ii) curves were fitted better without a slope parameter.

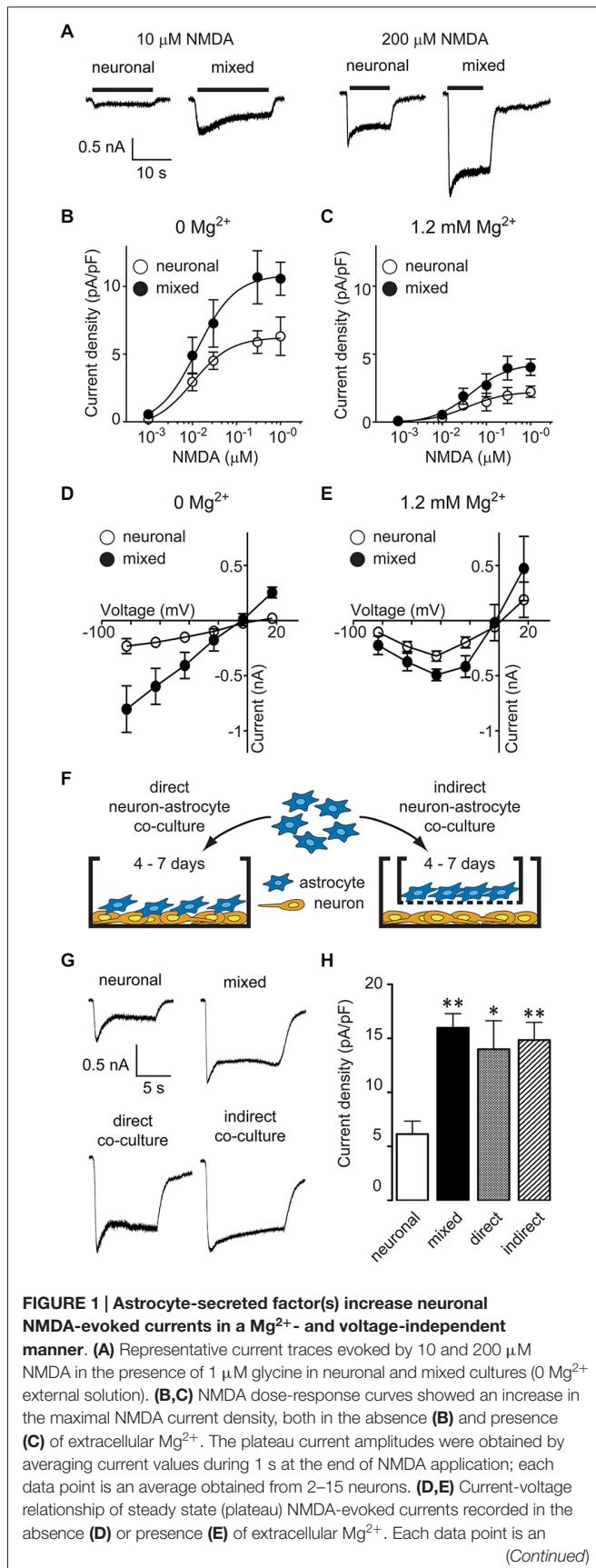
To determine weighted mean unitary conductance, MATLAB (MathWorks) was used to perform fluctuation analysis on the slowly decaying whole-cell currents evoked by 5 μM NMDA in the presence of 1 μM glycine. (To achieve the sufficiently slow current decay, the wash in these experiments was performed through a whole bath solution exchange rather than through the fast perfusion system used in other experiments.) The mean current and noise variance were calculated from adjacent 500 ms intervals during the portion of the current decay phase that was well fitted with a single exponential; to minimize the effect of changing current amplitude, the current variance was determined after subtracting this single exponential fit from the raw current trace. The mean current-variance plots showed a linear relationship, indicating that only a small fraction of the available channels were open; the weighted mean unitary current was determined from the slope of the linear fit (Watt et al., 2000). The weighted mean single channel conductance was obtained by dividing the mean unitary current by the driving force (−68.8 mV).

Statistical analyses were performed with GraphPad Prism statistical software; the specific test used for each experiment was chosen based on the experimental design and is specified in the main text and figure legends. The data are shown as mean ± SEM, unless indicated otherwise; *p* < 0.05 was considered statistically significant.

Results

In Hippocampal Cultures with Mature Synapses, Astrocytes Increase Postsynaptic NMDAR Current Density Through Secretion of a Soluble Factor (or Factors)

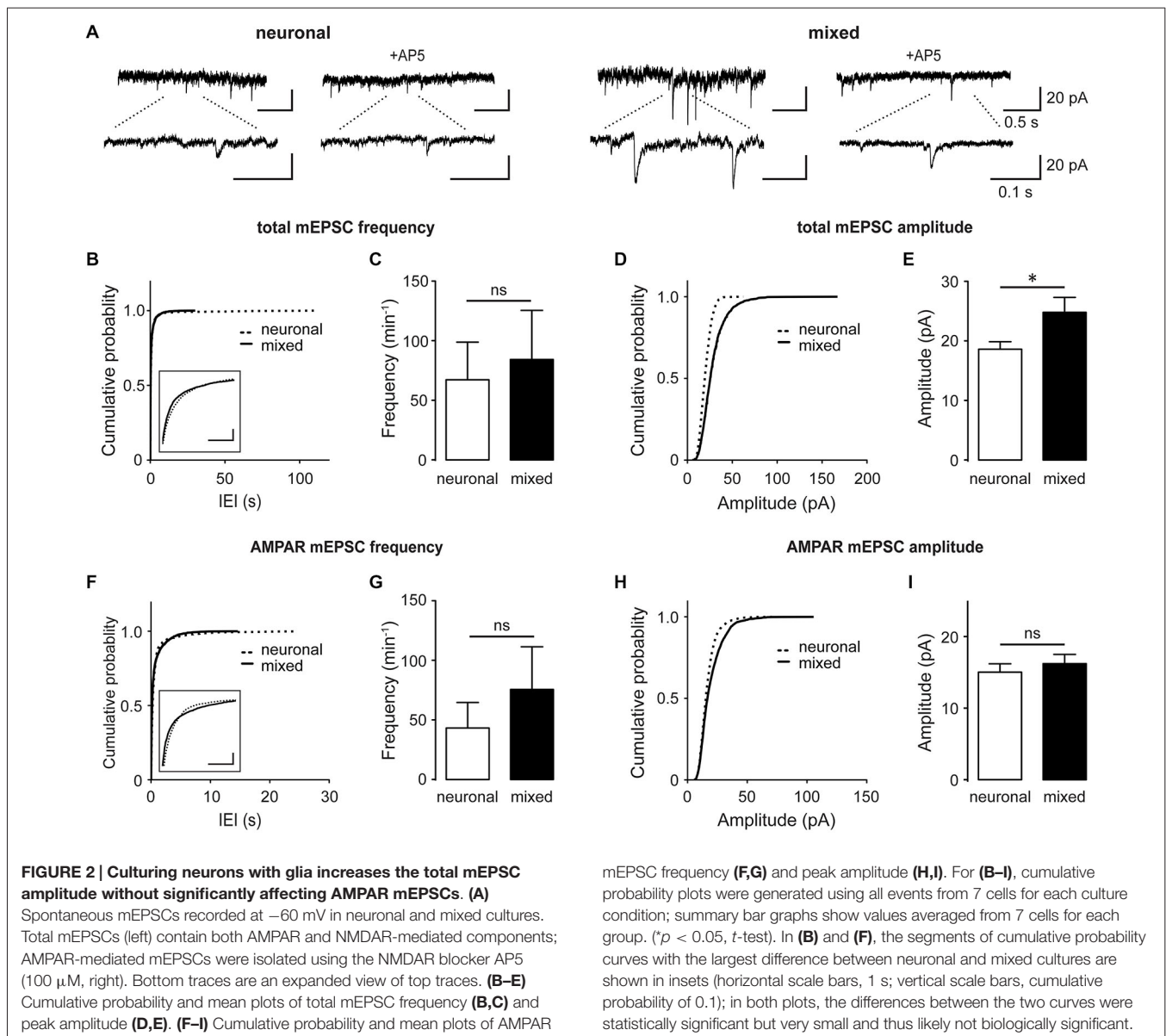
To investigate the effect of glia on neuronal NMDARs, we compared NMDAR activity between mixed and predominantly neuronal primary hippocampal cultures by recording whole-cell currents evoked by bath application of NMDA in the presence of glycine, with or without extracellular Mg²⁺. [In our culture system, the neuron-glia ratio is approximately 50%–50% in mixed cultures and 95%–5% in AraC-treated, neuron-enriched cultures; for images of each culture condition, see Habas et al. (2013)]. NMDA-evoked currents were larger in mixed than in neuronal cultures; representative traces from recordings in 0 mM Mg²⁺ are shown in **Figure 1A**. To examine NMDA current differences in a systematic way, we constructed dose-response curves (Eq. 1) for steady-state current density (plateau current normalized by cell capacitance; **Figures 1B,C**). NMDA *EC*₅₀ values did not significantly differ between the two culture conditions (0 Mg²⁺: 13 μM in mixed vs. 10 μM in neuronal cultures; 1.2 mM Mg²⁺: 44 μM in mixed vs. 39 μM in neuronal cultures; *p* > 0.05, *F*-test) and were comparable to values previously reported in the literature [7–16 μM in Mg²⁺-free and 25–40 μM in Mg²⁺-containing

**FIGURE 1 | Continued**

average obtained from 3–8 neurons. (F) A schematic diagram of the two neuron-astrocyte co-culture arrangements used for experiments. In direct co-cultures (left), astrocytes were plated directly onto AraC-treated neuronal cultures. In indirect co-cultures, astrocytes were plated on culture inserts that were then placed into wells with AraC-treated neuronal cultures; the insert membrane (1 μm pore size) allowed free exchange of soluble factors but prevented a direct contact between the two cell types. (G) Representative current traces evoked by 100 μM NMDA in the presence of 1 μM glycine in neuronal cultures, mixed cultures, direct neuron-astrocyte co-cultures, and indirect neuron-astrocyte co-cultures. (H) The average NMDA-evoked current density was significantly larger in mixed cultures and astrocyte co-cultures compared to neuronal cultures ($*p < 0.05$, $**p < 0.01$; one-way ANOVA with Dunnett post-test).

recording solutions (Verdoorn and Dingledine, 1988; Patneau and Mayer, 1990; Dildy-Mayfield and Leslie, 1991; Jaekel et al., 2006; Linsenhardt et al., 2013)]. In contrast, the maximal NMDAR current density was two-fold greater in mixed than neuronal cultures regardless of the Mg^{2+} concentration used (0 Mg^{2+} : 10.6 ± 1.2 pA/pF vs. 6.3 ± 1.4 pA/pF; 1.2 mM Mg^{2+} : 4.0 ± 0.6 pA/pF vs. 2.2 ± 0.4 pA/pF, $p < 0.05$, F -test). Since the voltage dependence of Mg^{2+} block shapes the voltage dependence of NMDAR currents (Nowak et al., 1984), this finding suggested that glial modulation of NMDARs was voltage independent; to investigate this further, we directly assessed the current-voltage (I-V) relationship of NMDA-evoked currents (Figures 1D,E). In Mg^{2+} -free recording solution (Figure 1D), I-V curves were linear with a reversal potential of ~ 0 mV in both culture conditions, as described previously (Nowak et al., 1984); however, the current amplitudes were significantly greater in mixed than neuronal cultures ($p < 0.0001$; two-way ANOVA). In the presence of 1.2 mM Mg^{2+} (Figure 1E), I-V curves exhibited a typical block at negative voltages while maintaining the significant amplitude difference between the two culture conditions ($p < 0.05$; two-way ANOVA).

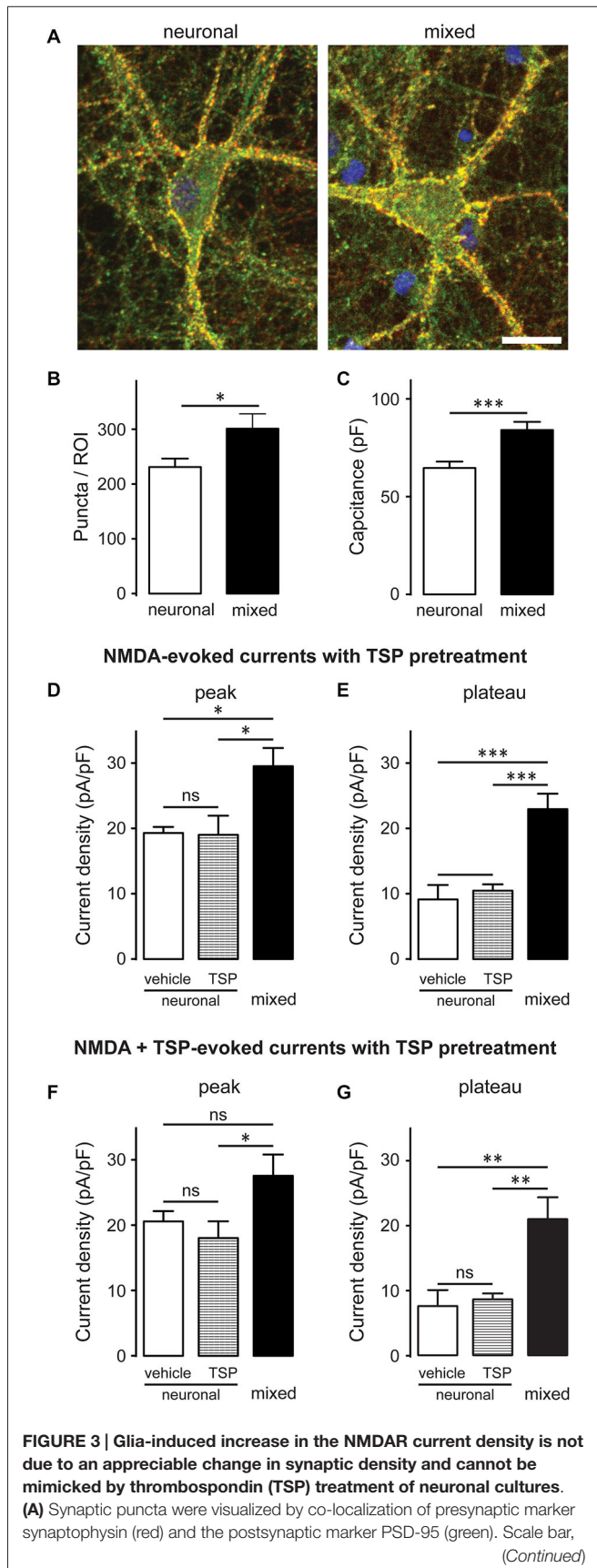
Mixed hippocampal cultures used in these experiments contain a heterogeneous population of glia. To determine whether the increase in neuronal NMDAR current density was mediated by astrocyte-secreted factor(s), we used two different modes of neuron-astrocyte co-culture, as described previously (Habas et al., 2013): in direct co-cultures, there was a physical contact between neurons and astrocytes, while in indirect co-cultures, the two cell types shared the same medium but were not in a direct contact (Figure 1F). The density of NMDAR currents evoked by 100 μM NMDA and 1 μM glycine (in the absence of Mg^{2+}) was comparable between mixed cultures (16.0 ± 1.3 pA/pF), direct neuron-astrocyte co-cultures (14.0 ± 2.6 pA/pF), and indirect neuron-astrocyte co-cultures (14.8 ± 1.6 pA/pF) and was approximately twice as large as the density of NMDAR currents in neuronal cultures (6.1 ± 1.2 pA/pF) (Figures 1G,H; one-way ANOVA with *post hoc* Dunnett test, $p < 0.01$, $p < 0.05$, and $p < 0.01$, respectively; $n = 8$). Taken together, these results demonstrate that astrocytes increase neuronal NMDAR current density in a voltage-independent fashion through a secretion of a soluble factor (or factors).



In the Presence of Astrocytes, there is an Increase in the Size of NMDAR-Mediated Synaptic Currents but No Significant Change in the Overall Synaptic Density

Several studies have shown that astrocyte-secreted factors regulate synapse formation and function during development of retinal ganglion cells (Pfrieger and Barres, 1997; Ullian et al., 2001; Christopherson et al., 2005; Allen et al., 2012), raising the possibility that the astrocyte-induced increase in the whole-cell NMDAR current density was a result of the increase in the overall synapse density. However, glial influence on excitatory synapses varies with neuronal cell type (Steinmetz et al., 2006) and developmental stage (Xu et al., 2010). To directly examine glial effect(s) on excitatory synapses in our hippocampal culture system, we recorded spontaneous synaptic

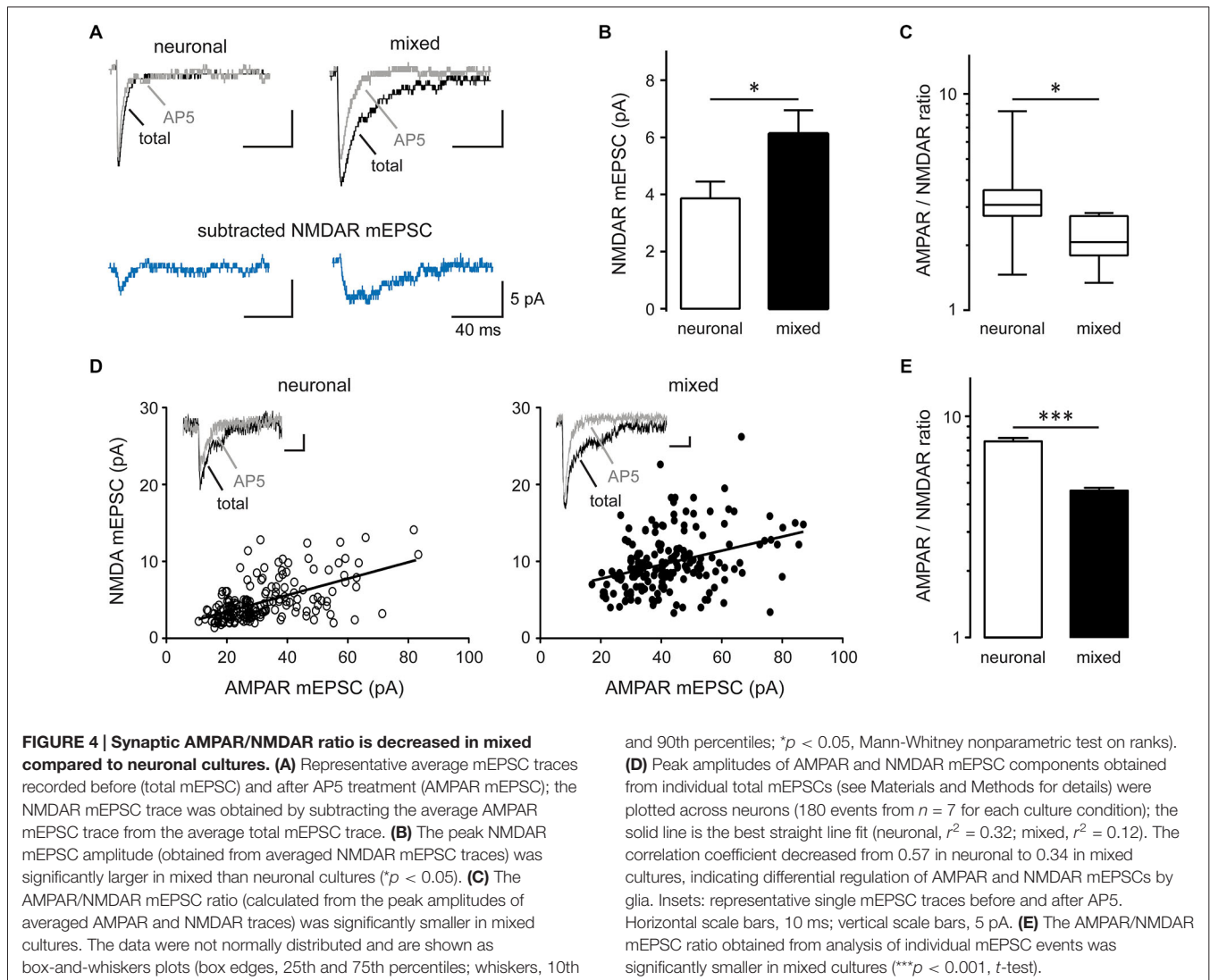
activity at DIV13–17, when synaptogenesis is known to reach a plateau (Grabrucker et al., 2009; Xu et al., 2010). Total miniature excitatory postsynaptic excitatory currents (mEPSCs), which contain both AMPAR- and NMDAR-mediated components, were recorded in the presence of 1 μ M tetrodotoxin (TTX) to block action potentials and 20 μ M bicuculline to block inhibitory synaptic transmission (**Figures 2A–E**). Cumulative probability plots of the mEPSC inter-event-interval (IEI; **Figure 2B**) and amplitude (**Figure 2D**) showed small but statistically significant changes in the overall event distribution (total mEPSC IEI: $p < 0.005$, total mEPSC amplitude: $p < 0.001$, Kolmogorov-Smirnov [KS] test); however, the mean mEPSC frequency did not significantly differ between the two culture conditions (84.3 ± 41.2 min^{-1} for mixed vs. 67.2 ± 31.6 min^{-1} for neuronal cultures, $n = 7$, $p = 0.6$, t -test; **Figure 2C**). In contrast,

**FIGURE 3 | Continued**

20 μm . **(B,C)** The number of synaptic puncta per ROI (which included the soma and proximal dendrites of each imaged neuron) was higher in mixed than neuronal cultures **(B)**; however, this increase was proportional to the increase in the neuronal membrane capacitance (a proxy for the neuronal surface area) observed in mixed cultures **(C)**. **(B,C)**: * $p < 0.05$, *** $p < 0.001$; t -test **(D,E)** 10-day pretreatment of neuronal cultures with 5 $\mu\text{g/ml}$ TSP had no effect on NMDAR current density measured at either peak or plateau time points; for comparison, NMDAR current density in mixed sister cultures was significantly larger than the current density in neuronal cultures after either pretreatment. Control neuronal cultures were pretreated with vehicle (0.07% glycerol); NMDA currents were evoked by application of 200 μM NMDA in the presence of glycine. **(F,G)** Acute TSP treatment (5 $\mu\text{g/ml}$) had no effect on NMDAR current density in neuronal cultures. In these experiments, neuronal cultures were first pretreated with 5 $\mu\text{g/ml}$ TSP or vehicle, as described for **(D,E)**; TSP or vehicle were then co-applied with NMDA in the presence of glycine. There was no difference in the mean NMDAR current density between TSP- and vehicle-treated cultures at either time point (peak and plateau); as expected, NMDAR current density was significantly larger in mixed sister cultures. **(D-G)**: * $p < 0.05$, ** $p < 0.01$, *** $p < 0.001$, one-way ANOVA with Bonferroni post-test).

the peak total mEPSC amplitude was 33% larger in mixed than neuronal cultures (24.8 ± 2.5 pA vs. 18.6 ± 1.3 pA respectively, $n = 7$, $p < 0.05$, t -test; **Figure 2E**). When recordings were performed in the presence of 100 μM AP5 to block the NMDAR mEPSC component (**Figures 2A,F-I**), we again observed very small but statistically significant changes in the distribution of AMPAR mEPSC IEI (**Figure 2F**) and amplitude (**Figure 2H**) ($p < 0.001$, KS test). However, there was no statistical significance in the mean frequency (76.4 ± 35.6 min^{-1} in mixed vs. 43.2 ± 22.0 min^{-1} in neuronal cultures, $n = 7$, $p > 0.05$, t -test; **Figure 2G**) or the mean peak amplitude of AMPAR mEPSCs between the two culture conditions (16.2 ± 1.3 pA in mixed vs. 15.0 ± 1.2 pA in neuronal cultures; $n = 7$, $p > 0.05$, t -test; **Figure 2I**).

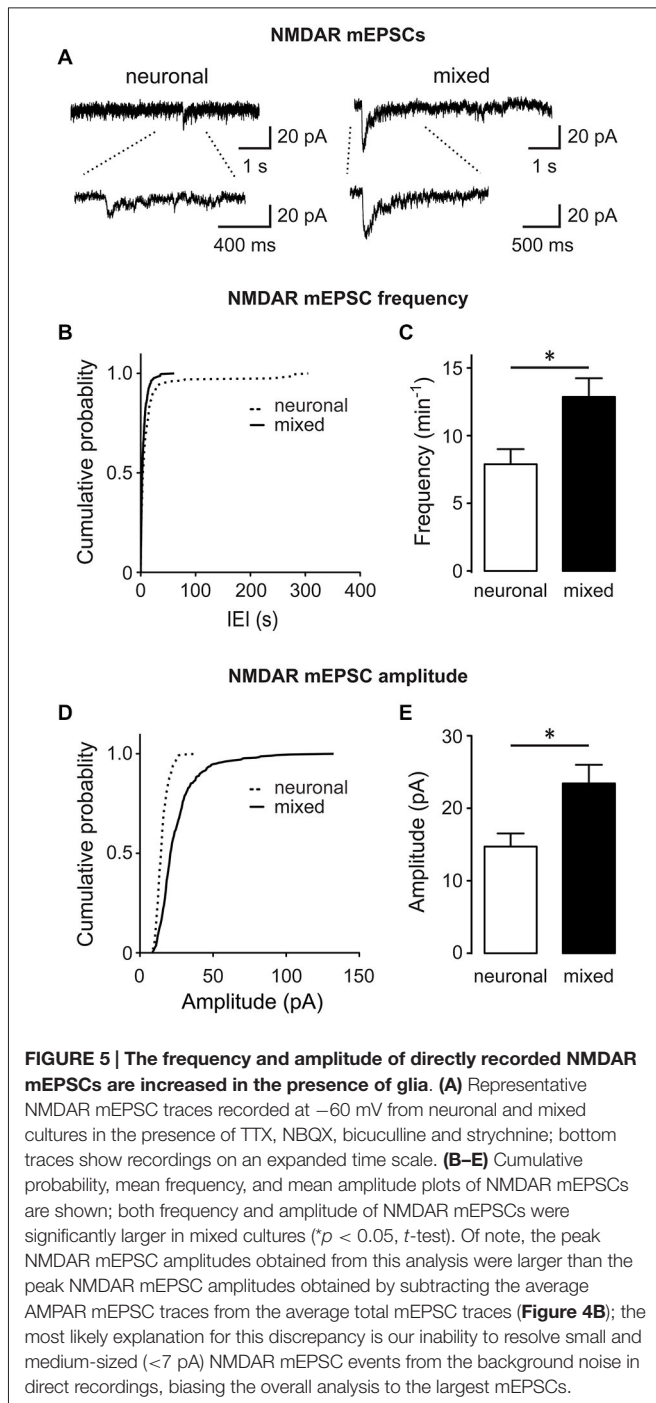
A subset of glutamatergic synapses contains only NMDARs (Hanse et al., 2013), rendering them AMPAR-silent and thus undetectable in standard mEPSC recordings; therefore, we also compared the overall number of synapses between the two culture conditions. Neurons were immunostained with antibodies against synaptophysin (a presynaptic marker; red) and PSD-95 (a postsynaptic marker; green), as described previously (Ullian et al., 2001; Christopherson et al., 2005; Ippolito and Eroglu, 2010); synapses were detected as yellow puncta, indicating co-localization of the two markers (**Figure 3A**). The number of synaptic puncta per ROI (which included the soma and proximal dendrites of imaged neurons) was 30% greater in mixed than neuronal cultures, a statistically significant difference (301.1 ± 27.2 vs. 231.2 ± 15.4 puncta/ROI; $n = 9$, $p < 0.05$, t -test; **Figure 3B**). However, neuronal surface area (measured as membrane capacitance) was also 30% greater in mixed than neuronal cultures (84.1 ± 4.2 pF vs. 64.7 ± 3.3 pF respectively, $n = 25$, $p < 0.001$, t -test; **Figure 3C**). These measurements were performed on different cell populations and thus could not be used for direct calculation of the number of synapses per unit of the membrane capacitance; nonetheless, together they strongly



suggest that synaptic density did not appreciably differ among the two culture conditions. In agreement with this finding, thrombospondin [astrocyte-secreted factor that promotes retinal ganglion cell synaptogenesis (Christopherson et al., 2005)] had no effect on the NMDAR current density in neuronal cultures (Figures 3D–G). Collectively, these data indicate that (i) the presence of glial cells does not have a major effect on the density of excitatory synapses in mature hippocampal cultures; and (ii) that the two-fold difference in whole-cell NMDAR current density between mixed and neuronal cultures cannot be explained by the difference in synaptic density between the two culture conditions.

The mean amplitude of total mEPSCs (Figure 2E), but not AMPAR mEPSCs (Figure 2I), was significantly larger in mixed than neuronal cultures, suggesting an increase in the NMDAR-mediated mEPSC component. Indeed, the mean amplitude of average NMDAR mEPSCs (obtained by subtraction of the average AMPAR mEPSC trace from the average total mEPSC trace for each neuron; Figure 4A) was significantly larger in

mixed than neuronal cultures (6.1 ± 0.8 vs. 3.9 ± 0.6 pA, respectively; $n = 7$, $p < 0.05$, t -test; Figure 4B), resulting in a decreased AMPAR/NMDAR ratio in mixed cultures (median of 2.1 in mixed vs. 3.1 in neuronal cultures, $n = 7$, $p < 0.05$, Mann-Whitney test; Figure 4C). To determine whether this increase in the average NMDAR mEPSC reflects a population of new synapses or an increase in the NMDAR mEPSC component of existing synapses, we examined the AMPAR/NMDAR ratio at individual synapses using kinetics analysis that is based on distinctive inactivation properties of these two types of glutamate receptors, as described previously (Edmonds et al., 1995; Watt et al., 2000). When NMDAR and AMPAR mEPSC amplitudes from each event were plotted against each other, the correlation coefficient became smaller in mixed cultures (0.34) than in neuronal cultures (0.57) (Figure 4D), indicating that AMPAR and NMDAR components of mEPSC were not proportionally scaled at individual synapses. In agreement with this observation and with the results from the average mEPSC analysis (Figures 4A–C),



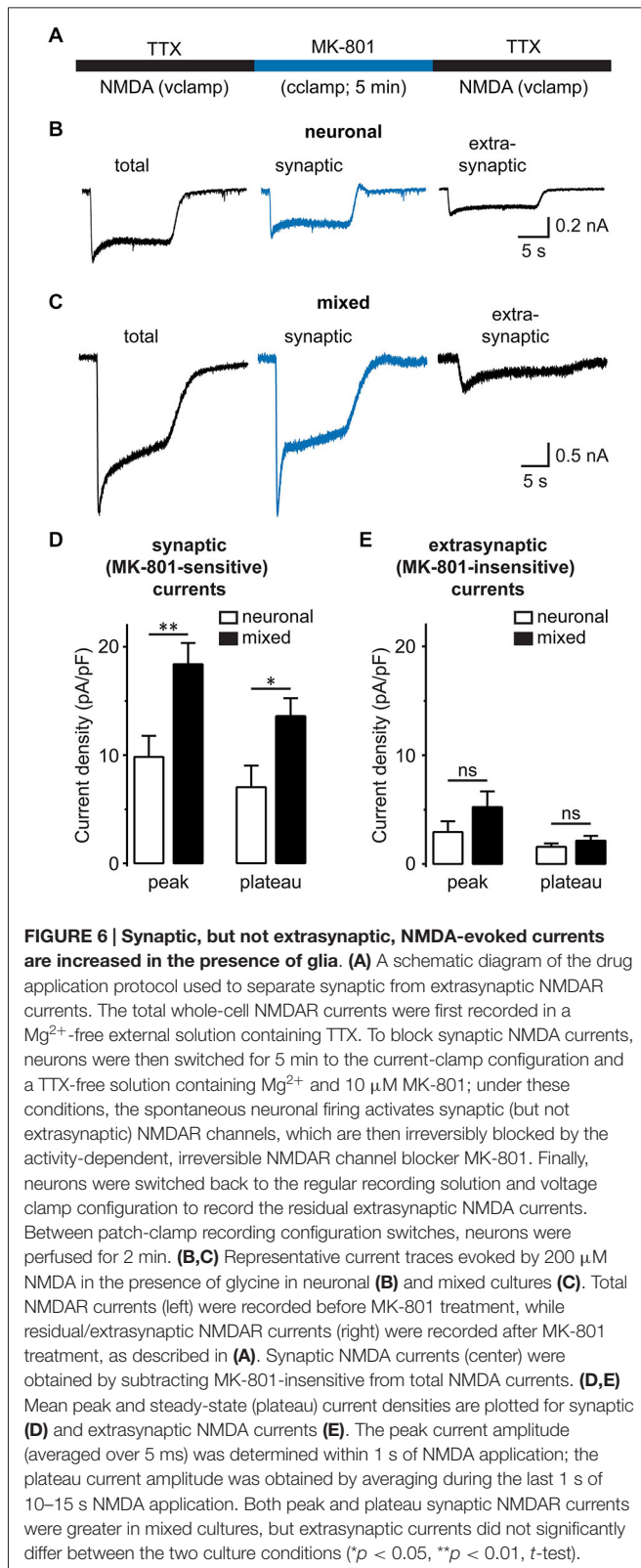
the AMPAR/NMDAR ratio obtained from individual mEPSCs was significantly smaller in mixed than neuronal cultures (4.6 ± 0.1 vs. 7.7 ± 0.3 , $n = 7$; $p < 0.001$, t -test; Figure 4E). To directly measure differences in NMDAR mEPSCs between mixed and neuronal cultures, we performed recordings in the presence of the AMPAR blocker NBQX ($10 \mu\text{M}$) in addition to TTX, bicuculline, and strychnine ($1 \mu\text{M}$) (Figure 5A). Cumulative plots of the NMDAR mEPSC IEI and amplitude showed a large and statistically significant change in the

overall event distribution (total mEPSC IEI: $p < 0.005$, total mEPSC amplitude: $p < 0.001$, KS test; Figures 5B,D). In addition, there was a significant increase in the NMDAR mEPSC frequency and peak amplitude in mixed compared to neuronal cultures (12.9 ± 1.4 vs. $7.9 \pm 1.1 \text{ min}^{-1}$ and 23.4 ± 2.6 vs. 14.0 ± 1.4 pA, $n = 6-7$, $p < 0.05$, t -test; Figures 5C,E). Taken together, these results demonstrate that (i) NMDAR-mediated synaptic currents in mature hippocampal neurons are potentiated in the presence of astrocytes and (ii) astrocytes differentially affect NMDARs and AMPARs at individual synapses, resulting in a lower AMPAR/NMDAR ratio in mixed cultures.

Astrocytes Selectively Regulate Synaptic GluN2B NMDARs

Synaptic and extrasynaptic NMDARs have a similar subunit composition, but different cellular functions (Hardingham and Bading, 2010). To determine whether glia differentially modulate these two NMDAR populations, we used the activity-dependent open NMDAR channel blocker MK-801 to isolate synaptic from extrasynaptic NMDAR currents, as described previously (Papadia et al., 2008): after synaptic NMDA currents were irreversibly blocked by MK-801 application during a period of spontaneous neuronal activity, residual extrasynaptic NMDAR currents were evoked by bath application of NMDA (Figure 6A; representative recordings from neuronal and mixed cultures are shown in Figures 6B,C). In agreement with the data from our mEPSC experiments, the density of the synaptic (MK-801-sensitive) NMDAR current was significantly greater in mixed cultures at both peak and plateau time points [peak: 18.4 ± 2.0 vs. 9.8 ± 1.9 pA/pF, $p < 0.01$; plateau: 13.5 ± 1.6 vs. 7.0 ± 2.0 pA/pF, $p < 0.05$; $n = 12-13$, t -test (Figure 6D)]. In contrast, the density of the extrasynaptic (MK-801-insensitive) NMDAR current did not significantly differ between the two culture conditions [peak: 5.2 ± 1.4 pA/pF in mixed vs. 2.9 ± 1.0 pA/pF in neuronal cultures, $p > 0.05$; plateau: 2.1 ± 0.4 in mixed vs. 1.6 ± 0.3 pA/pF in neuronal cultures, $p > 0.05$; $n = 12-13$, t -test (Figure 6E)].

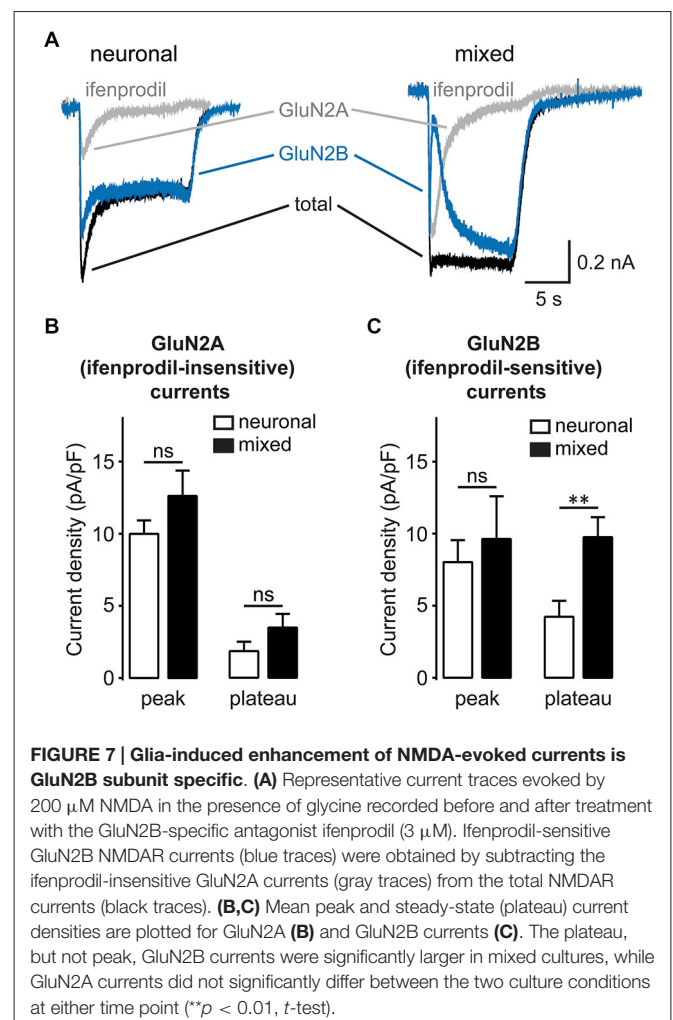
A significant fraction of the synaptic NMDAR current is carried by channels that incorporate slowly-inactivating GluN2B subunit, although these channels are found at both subcellular locations (Harris and Pettit, 2007). To examine the subunit specificity of glial NMDAR potentiation, we recorded NMDA-evoked currents in the presence of ifenprodil ($3 \mu\text{M}$), a GluN2B-selective inhibitor (Williams, 1993; Figure 7A). The density of ifenprodil-insensitive, largely GluN2A-mediated NMDAR currents was not significantly different between the two culture conditions [peak: 12.6 ± 1.8 pA/pF in mixed vs. 10.0 ± 0.9 pA/pF in neuronal cultures, $p > 0.05$; plateau: 3.5 ± 1.0 pA/pF in mixed vs. 1.8 ± 0.7 pA/pF in neuronal cultures, $p > 0.05$; $n = 8-10$, t -test (Figure 7B)]. In contrast, ifenprodil-sensitive, GluN2B-mediated currents were significantly larger in mixed cultures when measured at the plateau, but not at the peak time point [peak: 9.6 ± 3.0 vs. 8.0 ± 1.5 pA/pF, $p > 0.05$; plateau: 9.8 ± 1.4 vs. 4.2 ± 1.1 pA/pF, $p < 0.001$; $n = 8-10$, t -test

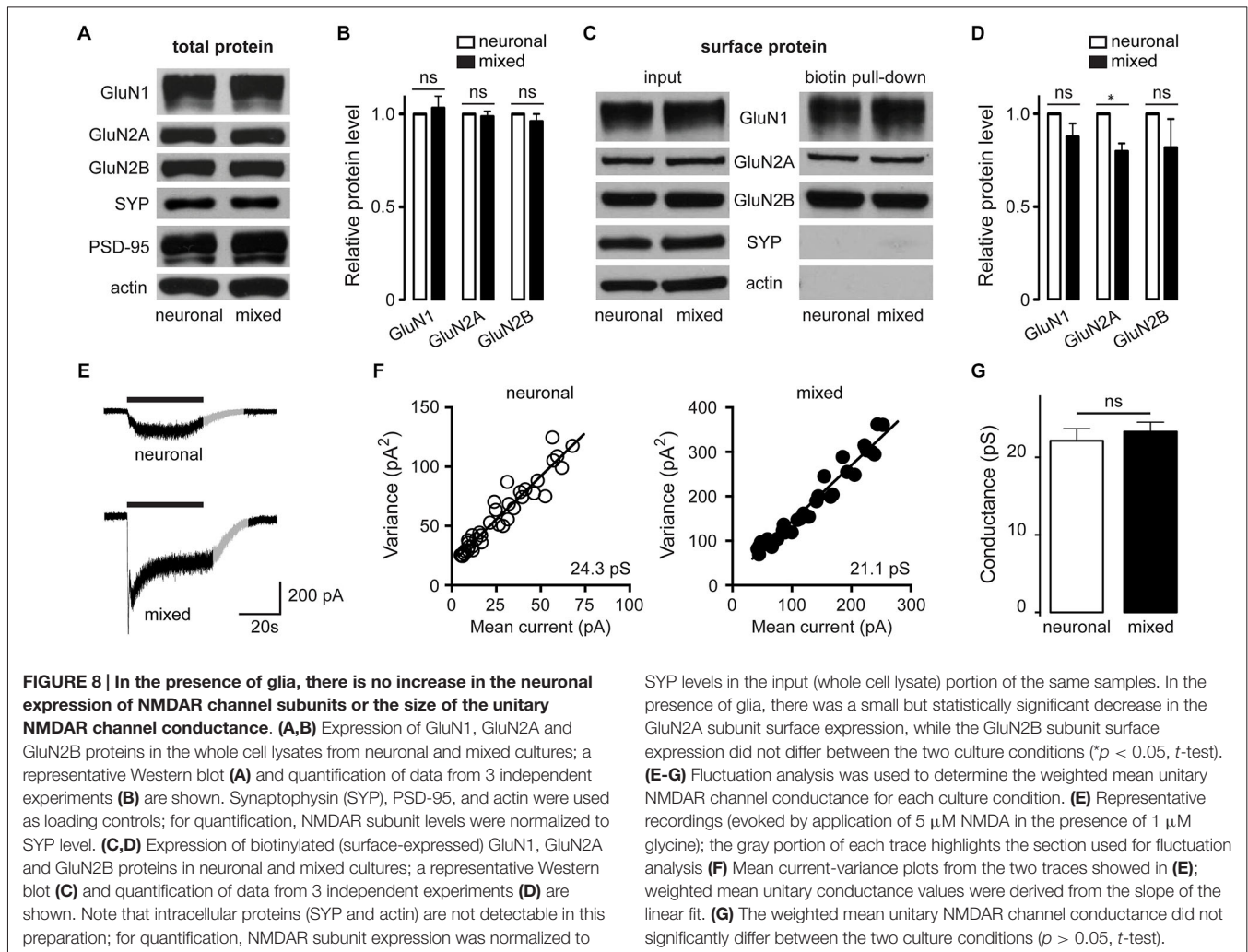


(Figure 7C)]. Taken together, these data indicate that synaptic GluN2B-containing NMDAR channels are the target of glial modulation.

Astrocytes Regulate NMDAR Channel Activity Through a PKC-Mediated Mechanism

Increased whole-cell current density can be due to an increase in the number of ion channels on the cell surface or to an increase in the activity of ion channels already localized to the plasma membrane. To differentiate between these two possibilities, we examined the total and cell surface expression of the major hippocampal NMDAR subunits, GluN1, GluN2A and GluN2B. In contrast to glial modulation of AMPAR [which involves increased cell surface expression and clustering of AMPAR GluA1 subunits (Allen et al., 2012)], neither total protein level nor cell surface expression of GluN1, GluN2A and GluN2B subunits was significantly higher in mixed compared to neuronal cultures (**Figures 8A–D**), indicating that the increase in the whole-cell current density was due to a change in the activity of the surface-expressed NMDAR channels. Ion channel activity is a function of two different aspects of single channel behavior: single channel (unitary) conductance and single channel kinetics. While evaluation of single channel kinetics requires patch recordings not suitable for analysis of physically inaccessible synaptic channels (Traynelis and Jaramillo, 1998),



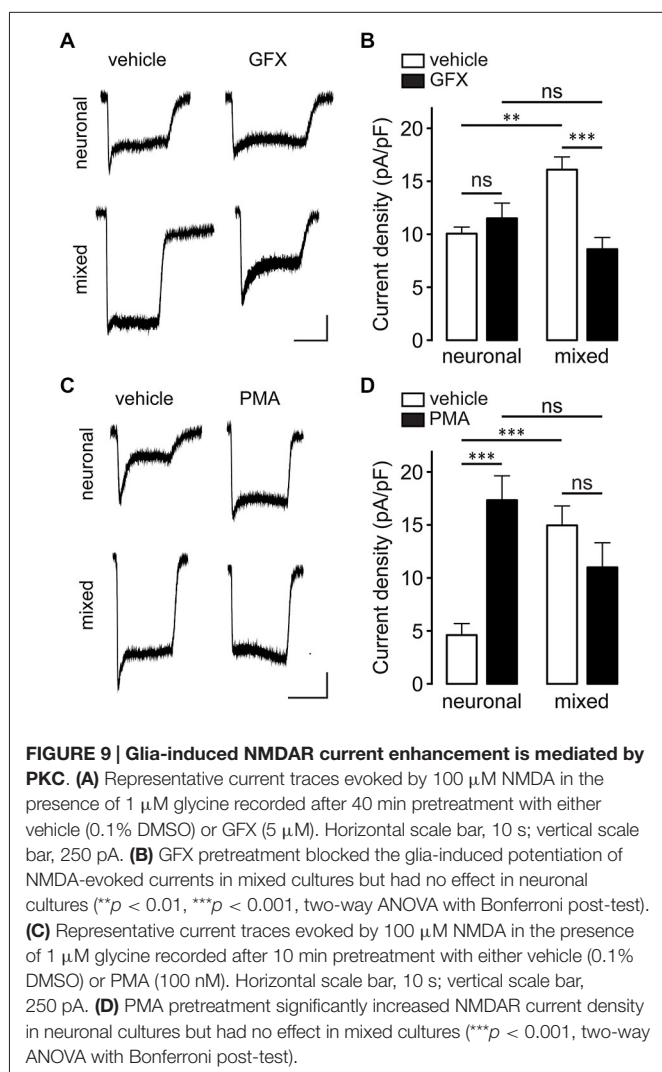


unitary conductance can be determined from fluctuation analysis of macroscopic currents (Sigworth, 1981). To further elucidate the mechanism mediating astrocytic enhancement of NMDAR channel activity, we therefore performed fluctuation analysis of the slowly decaying whole-cell currents evoked by 5 μ M NMDA (Mayer et al., 1988; Watt et al., 2000). **Figures 8E,F** show representative current traces and mean current-variance plots for one neuron from each culture condition, with the slope of the linear fit yielding the weighted mean unitary conductances of 24.3 pS (neuron without glia) and 21.1 pS (neuron with glia) for the two neurons shown; these values are smaller than the NMDAR conductance values obtained from outside-out patch recordings [40–50 pS (Jahr and Stevens, 1987; Ascher et al., 1988; Robinson et al., 1991)], but are in line with a broad range of NMDAR single channel conductance values obtained from fluctuation analysis [9–41 pS (Ascher et al., 1988; Sah et al., 1989; Watt et al., 2000)]. Importantly, the mean weighted unitary NMDAR channel conductance did not significantly differ between the two culture conditions (22.2 ± 1.5 pS in neuronal vs. 23.3 ± 1.2 pS in mixed cultures, $n = 6-7$, $p > 0.05$, *t*-test; **Figure 8G**), suggesting

that a change in the single channel kinetics rather than a change in the single channel conductance is the key biophysical mechanism mediating the astrocytic modulation of synaptic GluN2B NMDAR channels.

PKC was previously shown to increase the whole-cell NMDAR current by phosphorylation of Ser1303 and/or Ser1323 in the C-terminus of GluN2B (Liao et al., 2001). To investigate whether PKC is involved in the astrocyte-induced potentiation of NMDAR currents, neuronal and mixed cultures were pretreated with PKC inhibitor GF 109203X (GFX; 5 μ M) for 40 min prior to recording (**Figures 9A,B**). [GFX inhibits PKC with IC_{50} of ~ 10 nM (Toullec et al., 1991), but in physiological experiments it is typically used at concentrations between 1–10 μ M.] GFX pretreatment significantly attenuated NMDAR current density in mixed cultures (16.1 ± 1.2 vs. 8.6 ± 1.1 pA/pF; $n = 6-10$, $p < 0.01$, two-way ANOVA with Bonferroni multiple comparison post-test) but had no effect in neuronal cultures (10.1 ± 0.6 vs. 11.5 ± 1.4 pA/pF; $p > 0.05$); as a result, the difference in NMDAR current density between the two culture types, which was significant in vehicle-pretreated cultures ($p < 0.01$), was completely abolished following GFX

pretreatment ($p > 0.05$). In agreement with these results, PKC activator phorbol-12-myristate-13-acetate (PMA) had the opposite effect (Figures 9C,D): pretreatment with 100 nM PMA significantly increased NMDAR current density in neuronal cultures (17.4 ± 2.3 vs. 4.6 ± 1.1 pA/pF; $n = 8-12$, $p < 0.001$, two-way ANOVA with Bonferroni multiple comparison post-test) but had no effect in mixed cultures (15.0 ± 1.8 vs. 11.0 ± 2.3 pA/pF; $p > 0.05$); consequently, the difference in NMDAR current density between the two culture types (which was significant in vehicle-pretreated cultures; $p < 0.001$) was not significant following PMA pretreatment ($p > 0.05$). Interestingly, however, there was no significant difference in the phosphorylation status of GluN2B Ser1303 between the two culture conditions in either vehicle- or GFX-treated cultures (Figure 10; phosphorylation of Ser1323 could not be evaluated due to the lack of phospho-specific antibodies targeting that site). Taken together, these data indicate that PKC mediates the astrocyte-induced increase in the synaptic GluN2B channel activity, but that this effect does not involve phosphorylation of GluN2B-Ser1303.

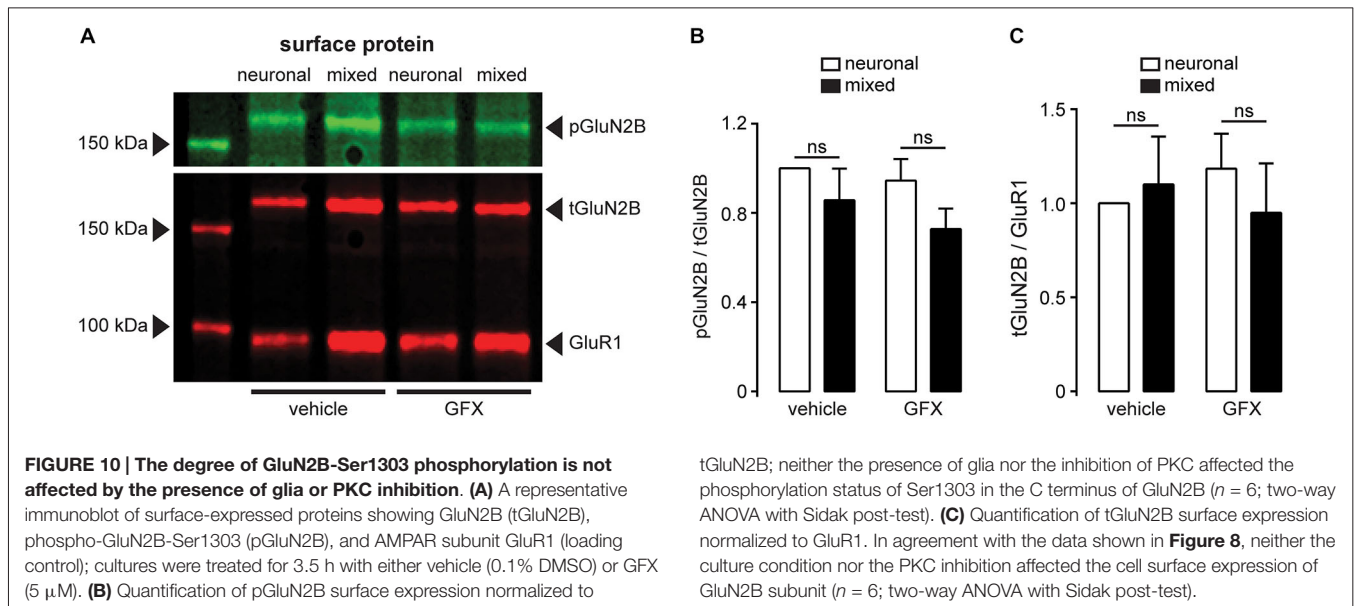


Discussion

Neuronal NMDARs play a critical role in synaptic plasticity, neuroprotection, and neurotoxicity, but relatively little is known about their regulation by glial cells. Our study identified a novel form of astrocytic NMDAR modulation that occurs in a subunit- and subcellular localization-dependent manner. The density of NMDA-evoked whole-cell current was approximately doubled in neurons cultured in the presence of a mixed population of glia compared to neurons cultured alone (Figure 1), indicating a change in either expression or function of postsynaptic NMDAR channels. The glial effect was mediated by (an) astrocyte-secreted soluble factor(s) (Figure 1), was Mg^{2+} and voltage independent (Figure 1), and could not be explained by an appreciable change in the synaptic density (Figure 3). Instead, we found that the peak amplitude of total and NMDAR mEPSCs, but not AMPAR mEPSCs, was significantly larger in mixed cultures, resulting in a decreased synaptic AMPAR/NMDAR ratio (Figures 2, 4, 5). Astrocytic modulation was restricted to synaptic NMDARs that contain the GluN2B subunit (Figures 6, 7), did not involve an increase in the cell surface expression of NMDAR subunits (Figure 8), and was mediated by PKC (Figure 9). Collectively, these data show that astrocyte-secreted soluble factor(s) can fine-tune synaptic NMDAR activity through the PKC-mediated regulation of GluN2B NMDAR channels already present at postsynaptic sites, presumably on a rapid time scale (Figure 11).

Based on studies of transgenic mice that express dominant negative SNARE (dnSNARE) construct under the control of a glial fibrillary acidic protein (GFAP) promoter, it was previously suggested that astrocytes regulate the surface expression of GluN2A and GluN2B subunits by increasing the extracellular concentration of adenosine, which activates A1 receptors and leads to tyrosine phosphorylation of Src kinase and the GluN2B subunit (Deng et al., 2011). However, these findings have been called in question by a recent study by Fujita et al., which showed that GFAP-dnSNARE mice (i) express dnSNARE not just in astrocytes but also in a subset of cortical and hippocampal neurons and (ii) do not exhibit increased extracellular concentration of adenosine *in vivo* (Fujita et al., 2014). We have not directly tested whether adenosine plays a role in the astrocytic modulation of synaptic GluN2B currents; however, using wild-type neurons and astrocytes, we have not observed a significant increase in the normalized surface expression of GluN2A and GluN2B subunits in mixed relative to neuronal cultures (Figures 8, 10). Our findings thus confirm that astrocytes regulate neuronal NMDAR channels, but suggest that the underlying mechanism does not involve changes in NMDAR subunit trafficking.

NMDAR currents are regulated by PKC in a complex manner; PKC-mediated NMDAR potentiation has been observed most often (Xiong et al., 1998; Lu et al., 1999; Zheng et al., 1999; Liao et al., 2001), but PKC-mediated suppression has also been reported (Markram and Segal, 1992). In the best studied form of PKC-mediated NMDAR current regulation, activation of G_q G protein-coupled (i.e., muscarinic M1 and glutamate mGluR5) receptors leads to activation

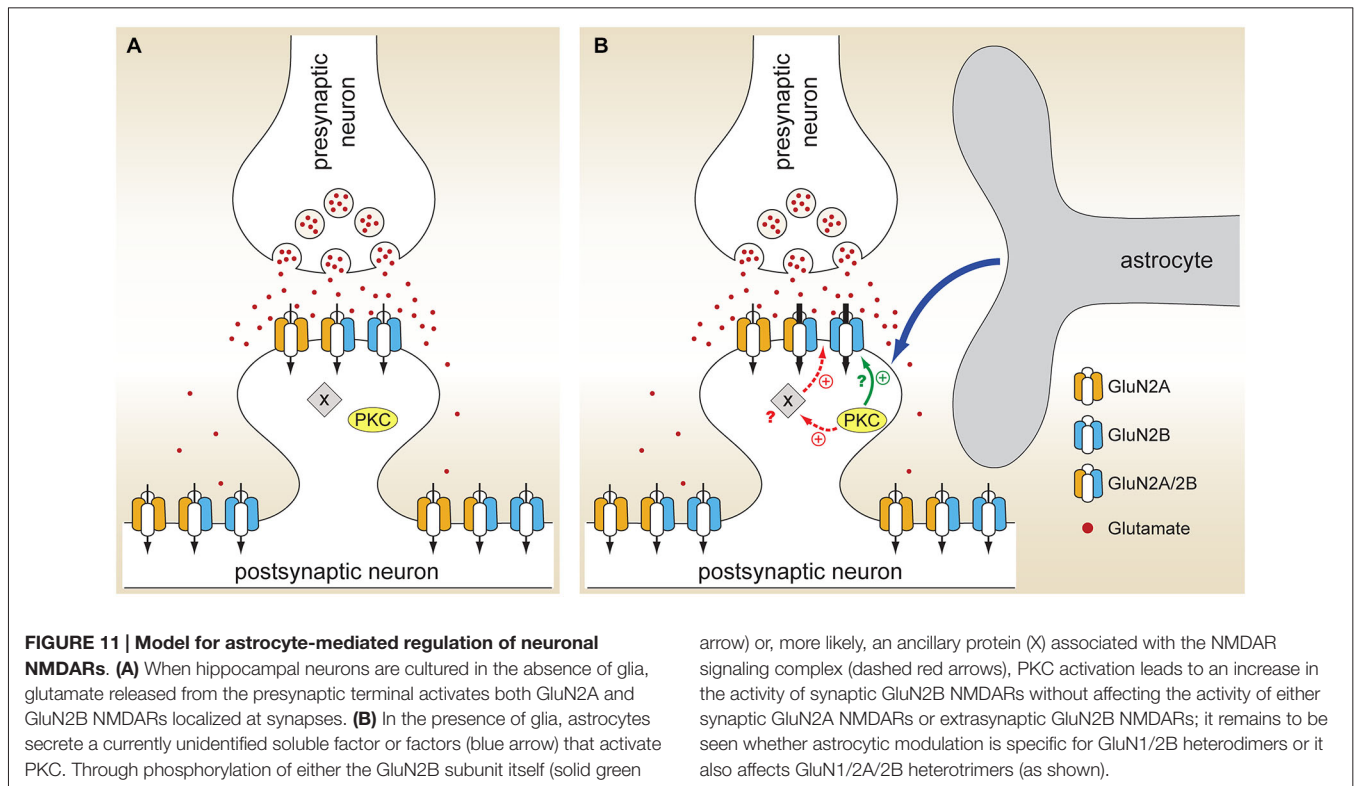


of the phospholipase C/PKC/Src kinase signaling cascade and enhancement of NMDA-evoked whole-cell currents that is greater at the peak than at the plateau (Lu et al., 1999, 2000). The preferential enhancement of peak NMDAR currents was originally interpreted as PKC regulation of Ca^{2+} -dependent inactivation (Lu et al., 1999), but is now understood as selective potentiation of GluN2A-containing NMDARs, which preferentially contribute to the peak NMDA-evoked currents (Yang et al., 2014). G_q /PKC/Src-mediated regulation of GluN2A NMDARs is thus distinct from the astrocyte-induced potentiation of GluN2B NMDARs reported in the current study, although both events seem to be mediated by a change in the single channel kinetics rather than a change in the single channel conductance [(Lu et al., 1999) and **Figure 8**]. It is not entirely clear why the PKC-mediated modulation of GluN2B NMDARs has not been observed in the earlier studies; however, it is worth noting that the previous work was performed in the absence of glia, largely using heterologous expression systems or acutely dissociated neurons. It is possible that astrocyte-secreted factors responsible for GluN2B NMDAR regulation activate PKC through a non-canonical, G_q G protein-independent mechanism that is yet to be elucidated.

What is the molecular target of PKC phosphorylation? Although both GluN1 and GluN2 subunits contain multiple PKC phosphorylation consensus sites (Chen and Roche, 2007), mutation or deletion of these sites does not completely eliminate PKC-mediated NMDAR current enhancement, suggesting that PKC effects are at least partly indirect (i.e., mediated by phosphorylation of other neuronal proteins). The C terminus of the GluN2B subunit contains two adjacent Ser residues (Ser1303 and Ser1323) that can be phosphorylated by PKC (Chen and Roche, 2007); Ser1303 is also phosphorylated by calcium/calmodulin-dependent protein kinase II (CaMKII) (Omkumar et al., 1996). In *Xenopus* oocytes, mutations of

Ser1303 and Ser1323 strongly attenuate, but do not completely block, the PKC modulation of recombinant GluN1/2B channels (Liao et al., 2001). We have not observed any difference in the phosphorylation status of Ser1303 between the two culture conditions either at baseline or following treatment with the PKC inhibitor GFX (**Figure 10**), indicating (i) that this residue is not involved in the astrocyte- and PKC-mediated modulation of synaptic GluN2B receptors and (ii) that in the intact neuronal milieu a kinase other than PKC (presumably CaMKII) has a dominant effect on Ser1303 phosphorylation. Additional work will be required to establish whether astrocyte-induced PKC activation leads to phosphorylation of a different residue within the GluN2B subunit or acts through an ancillary protein that is part of the NMDAR signaling complex (**Figure 11**). Notably, astrocytic regulation is restricted to synaptic GluN2B receptors (**Figures 6, 7**); given that GluN2B receptors can move between synaptic and extrasynaptic sites (Groc et al., 2006), it is not currently clear how this specificity is achieved. Most likely, kinases, phosphatases, and other signaling proteins that make up the supramolecular NMDA receptor complex differ between synaptic and extrasynaptic sites, and the differences in this subcellular environment play a role in the regulation of NMDAR channel activity.

What is the functional significance of synaptic GluN2B receptor regulation by astrocytes? At the early stages of postnatal development, there is a change in the neuronal NMDAR composition: GluN2B-containing NMDARs, which are the main NMDAR subtype expressed at birth, are partially replaced by GluN2A-containing NMDARs, which have a lower glutamate affinity and exhibit faster inactivation kinetics (Paoletti et al., 2013). This GluN2A-2B switch coincides with synaptic maturation; however, synapses with high GluN2A to GluN2B ratio require stronger stimulation to undergo long term potentiation (LTP; Paoletti et al., 2013). Thus, the GluN2A-2B switch is likely to have a negative effect on learning and



memory. In agreement with this hypothesis, overexpression of the GluN2B subunit in the adult forebrain leads to more robust LTP and enhanced performance on various learning and memory tasks in both mice (Tang et al., 1999) and rats (Wang et al., 2009), even at an old age (Cao et al., 2007). Of greater physiological relevance, transgenic mice with high serum levels of the anti-aging factor *klotho* show an increase in the GluN2B portion of synaptic NMDAR currents, which is accompanied by enhanced LTP and better performance on tests of learning and memory; in humans, heterozygosity for a lifespan-extending variant of the *KLOTHO* gene is associated with increased *klotho* serum levels and better cognition (Dubal et al., 2014). While *klotho* appears to regulate the number of GluN2B receptors expressed at synapses (Dubal et al., 2014), a similar learning enhancement would be expected to result from an astrocyte-mediated increase in the activity of GluN2B NMDARs that are already present at postsynaptic sites. We therefore propose that astrocytes can dynamically regulate the synaptic GluN2A/2B current ratio and the threshold for LTP induction; identification of the astrocyte-secreted factor(s) that mediate(s) NMDAR regulation will enable the direct testing of this hypothesis.

Ca^{2+} influx through synaptic NMDARs leads to activation of FOXO, C/EBP β , and AP-1 signaling pathways that together have a neuroprotective effect (Papadia et al., 2008). In contrast, activation of extrasynaptic NMDARs is generally neurotoxic (Hardingham et al., 2002). GluN2A- and GluN2B-containing NMDARs were originally hypothesized to preferentially signal to cell survival and cell death cascades, respectively (Liu

et al., 2007); however, later studies have demonstrated that either receptor subtype can activate both neuroprotective and neurotoxic signaling pathways (von Engelhardt et al., 2007; Martel et al., 2009). More recently, it has been shown that the C terminus of GluN2B is more effective than the C terminus of GluN2A in promoting neuronal death; however, this effect was observed when both synaptic and extrasynaptic NMDARs were chronically activated (Martel et al., 2012). In contrast, trans-synaptic (physiologic) activation of GluN2B receptors was shown to be neuroprotective (Papadia et al., 2008; Martel et al., 2009). Interestingly, we have found that astrocyte-secreted factor(s) selectively increase the current flow through synaptic, but not extrasynaptic, GluN2B-containing NMDARs. In the setting of physiologic synaptic activity, the astrocyte-mediated increase in the synaptic GluN2B receptor activity would thus be expected to have a net neuroprotective effect.

In summary, we have shown that astrocyte-secreted soluble factor(s) can fine-tune the activity of synaptic GluN2B NMDAR channels. Through this presumably rapid and reversible PKC-mediated molecular mechanism, astrocytes can regulate synaptic AMPAR/NMDAR and GluN2A/2B ratios without altering the expression or trafficking of NMDAR channel subunits. Elucidating the details of the signal transduction pathway that mediates astrocytic regulation of synaptic GluN2B channels thus has a potential to foster the development of pharmacologic treatments that will enhance cognitive performance while strengthening neuroprotective signaling.

Acknowledgments

This work was supported by National Institutes of Health grants NS054113 and NS073765 to MM. We thank Drs. Eric Ullian, Peter Sargent, Lily Jan, and Raymond Swanson for insightful

discussions at different stages of the project, Dr. Gunsoo Kim for technical help with fluctuation analysis, Dr. Robert Krencik for advice on synapse quantification, Mr. Vien Nguyen for assistance with early experiments, and Ms. Christine Lin for help with figure preparation.

References

- Allen, N. J., Bennett, M. L., Foo, L. C., Wang, G. X., Chakraborty, C., Smith, S. J., et al. (2012). Astrocyte glypicans 4 and 6 promote formation of excitatory synapses via GluA1 AMPA receptors. *Nature* 486, 410–414. doi: 10.1038/nature11059
- Ascher, P., Bregestovski, P., and Nowak, L. (1988). N-methyl-D-aspartate-activated channels of mouse central neurones in magnesium-free solutions. *J. Physiol.* 399, 207–226.
- Cao, X., Cui, Z., Feng, R., Tang, Y. P., Qin, Z., Mei, B., et al. (2007). Maintenance of superior learning and memory function in NR2B transgenic mice during ageing. *Eur. J. Neurosci.* 25, 1815–1822. doi: 10.1111/j.1460-9568.2007.05431.x
- Chen, B. S., and Roche, K. W. (2007). Regulation of NMDA receptors by phosphorylation. *Neuropharmacology* 53, 362–368. doi: 10.1016/j.neuropharm.2007.05.018
- Christopherson, K. S., Ullian, E. M., Stokes, C. C., Mallowney, C. E., Hell, J. W., Agah, A., et al. (2005). Thrombospondins are astrocyte-secreted proteins that promote CNS synaptogenesis. *Cell* 120, 421–433. doi: 10.1016/j.cell.2004.12.020
- Cull-Candy, S., Brickley, S., and Farrant, M. (2001). NMDA receptor subunits: diversity, development and disease. *Curr. Opin. Neurobiol.* 11, 327–335. doi: 10.1016/s0959-4388(00)00215-4
- Cull-Candy, S. G., and Leszkiewicz, D. N. (2004). Role of distinct NMDA receptor subtypes at central synapses. *Sci. STKE* 2004:re16. doi: 10.1126/stke.2552004re16
- Deng, Q., Terunuma, M., Fellin, T., Moss, S. J., and Haydon, P. G. (2011). Astrocytic activation of A1 receptors regulates the surface expression of NMDA receptors through a Src kinase dependent pathway. *Glia* 59, 1084–1093. doi: 10.1002/glia.21181
- Dildy-Mayfield, J. E., and Leslie, S. W. (1991). Mechanism of inhibition of N-methyl-D-aspartate-stimulated increases in free intracellular Ca^{2+} concentration by ethanol. *J. Neurochem.* 56, 1536–1543. doi: 10.1111/j.1471-4159.1991.tb02048.x
- Dubal, D. B., Yokoyama, J. S., Zhu, L., Broestl, L., Worden, K., Wang, D., et al. (2014). Life extension factor klotho enhances cognition. *Cell Rep.* 7, 1065–1076. doi: 10.1016/j.celrep.2014.03.076
- Edmonds, B., Gibb, A. J., and Colquhoun, D. (1995). Mechanisms of activation of glutamate receptors and the time course of excitatory synaptic currents. *Annu. Rev. Physiol.* 57, 495–519. doi: 10.1146/annurev.physiol.57.1.495
- Fellin, T., Halassa, M. M., Terunuma, M., Succol, F., Takano, H., Frank, M., et al. (2009). Endogenous nonneuronal modulators of synaptic transmission control cortical slow oscillations *in vivo*. *Proc. Natl. Acad. Sci. U S A* 106, 15037–15042. doi: 10.1073/pnas.0906419106
- Fu, Z., Logan, S. M., and Vicini, S. (2005). Deletion of the NR2A subunit prevents developmental changes of NMDA-mEPSCs in cultured mouse cerebellar granule neurones. *J. Physiol.* 563, 867–881. doi: 10.1113/jphysiol.2004.079467
- Fujita, T., Chen, M. J., Li, B., Smith, N. A., Peng, W., Sun, W., et al. (2014). Neuronal transgene expression in dominant-negative SNARE mice. *J. Neurosci.* 34, 16594–16604. doi: 10.1523/JNEUROSCI.2585-14.2014
- Grabrucker, A., Vaida, B., Bockmann, J., and Boeckers, T. M. (2009). Synaptogenesis of hippocampal neurons in primary cell culture. *Cell Tissue Res.* 338, 333–341. doi: 10.1007/s00441-009-0881-z
- Groc, L., Heine, M., Cousins, S. L., Stephenson, F. A., Lounis, B., Cognet, L., et al. (2006). NMDA receptor surface mobility depends on NR2A-2B subunits. *Proc. Natl. Acad. Sci. U S A* 103, 18769–18774. doi: 10.1073/pnas.0605238103
- Habas, A., Hahn, J., Wang, X., and Margeta, M. (2013). Neuronal activity regulates astrocytic Nrf2 signaling. *Proc. Natl. Acad. Sci. U S A* 110, 18291–18296. doi: 10.1073/pnas.1208764110
- Han, K. S., Woo, J., Park, H., Yoon, B. J., Choi, S., and Lee, C. J. (2013). Channel-mediated astrocytic glutamate release via Bestrophin-1 targets synaptic NMDARs. *Mol. Brain* 6:4. doi: 10.1186/1756-6606-6-4
- Hanse, E., Seth, H., and Riebe, I. (2013). AMPA-silent synapses in brain development and pathology. *Nat. Rev. Neurosci.* 14, 839–850. doi: 10.1038/nrn3642
- Hardingham, G. E., and Bading, H. (2003). The Yin and Yang of NMDA receptor signalling. *Trends Neurosci.* 26, 81–89. doi: 10.1016/s0166-2236(02)00040-1
- Hardingham, G. E., and Bading, H. (2010). Synaptic versus extrasynaptic NMDA receptor signalling: implications for neurodegenerative disorders. *Nat. Rev. Neurosci.* 11, 682–696. doi: 10.1038/nrn2911
- Hardingham, G. E., Fukunaga, Y., and Bading, H. (2002). Extrasynaptic NMDARs oppose synaptic NMDARs by triggering CREB shut-off and cell death pathways. *Nat. Neurosci.* 5, 405–414. doi: 10.1038/nn835
- Harris, A. Z., and Pettit, D. L. (2007). Extrasynaptic and synaptic NMDA receptors form stable and uniform pools in rat hippocampal slices. *J. Physiol.* 584, 509–519. doi: 10.1113/jphysiol.2007.137679
- Haydon, P. G., and Carmignoto, G. (2006). Astrocyte control of synaptic transmission and neurovascular coupling. *Physiol. Rev.* 86, 1009–1031. doi: 10.1152/physrev.00049.2005
- Ippolito, D. M., and Eroglu, C. (2010). Quantifying synapses: an immunocytochemistry-based assay to quantify synapse number. *J. Vis. Exp.* 45:e2270. doi: 10.3791/2270
- Jaekel, B., Mühlberg, K., Garcia de Arriba, S., Reichenbach, A., Verdager, E., Pallas, M., et al. (2006). Neuroprotection associated with alternative splicing of NMDA receptors in rat cortical neurons. *Br. J. Pharmacol.* 147, 622–633. doi: 10.1038/sj.bjp.0706471
- Jahr, C. E., and Stevens, C. F. (1987). Glutamate activates multiple single channel conductances in hippocampal neurons. *Nature* 325, 522–525. doi: 10.1038/325522a0
- Lee, C. J., Mannaioni, G., Yuan, H., Woo, D. H., Gingrich, M. B., and Traynelis, S. F. (2007). Astrocytic control of synaptic NMDA receptors. *J. Physiol.* 581, 1057–1081. doi: 10.1113/jphysiol.2007.130377
- Liao, G. Y., Wagner, D. A., Hsu, M. H., and Leonard, J. P. (2001). Evidence for direct protein kinase-C mediated modulation of N-methyl-D-aspartate receptor current. *Mol. Pharmacol.* 59, 960–964. doi: 10.1124/mol.59.5.960
- Linsenbardt, A. J., Chisari, M., Yu, A., Shu, H. J., Zorumski, C. F., and Mennerick, S. (2013). Noncompetitive, voltage-dependent NMDA receptor antagonism by hydrophobic anions. *Mol. Pharmacol.* 83, 354–366. doi: 10.1124/mol.112.081794
- Liu, Y., Wong, T. P., Aarts, M., Rooyackers, A., Liu, L., Lai, T. W., et al. (2007). NMDA receptor subunits have differential roles in mediating excitotoxic neuronal death both *in vitro* and *in vivo*. *J. Neurosci.* 27, 2846–2857. doi: 10.1523/jneurosci.0116-07.2007
- Lu, W. Y., Jackson, M. F., Bai, D., Orser, B. A., and MacDonald, J. F. (2000). In CA1 pyramidal neurons of the hippocampus protein kinase C regulates calcium-dependent inactivation of NMDA receptors. *J. Neurosci.* 20, 4452–4461.
- Lu, W. Y., Xiong, Z. G., Lei, S., Orser, B. A., Dudek, E., Browning, M. D., et al. (1999). G-protein-coupled receptors act via protein kinase C and Src to regulate NMDA receptors. *Nat. Neurosci.* 2, 331–338. doi: 10.1038/7243
- Markram, H., and Segal, M. (1992). Activation of protein kinase C suppresses responses to NMDA in rat CA1 hippocampal neurones. *J. Physiol.* 457, 491–501. doi: 10.1113/jphysiol.1992.sp019389
- Martel, M. A., Ryan, T. J., Bell, K. F., Fowler, J. H., McMahon, A., Al-Mubarak, B., et al. (2012). The subtype of GluN2 C-terminal domain determines the response to excitotoxic insults. *Neuron* 74, 543–556. doi: 10.1016/j.neuron.2012.03.021
- Martel, M. A., Wyllie, D. J., and Hardingham, G. E. (2009). In developing hippocampal neurons, NR2B-containing N-methyl-D-aspartate receptors (NMDARs) can mediate signaling to neuronal survival and synaptic

- potentiation, as well as neuronal death. *Neuroscience* 158, 334–343. doi: 10.1016/j.neuroscience.2008.01.080
- Mayer, M. L., Westbrook, G. L., and Vyklicky, L. Jr. (1988). Sites of antagonist action on N-methyl-D-aspartic acid receptors studied using fluctuation analysis and a rapid perfusion technique. *J. Neurophysiol.* 60, 645–663.
- Nowak, L., Bregestovski, P., Ascher, P., Herbet, A., and Prochiantz, A. (1984). Magnesium gates glutamate-activated channels in mouse central neurones. *Nature* 307, 462–465. doi: 10.1038/307462a0
- Om Kumar, R. V., Kiely, M. J., Rosenstein, A. J., Min, K. T., and Kennedy, M. B. (1996). Identification of a phosphorylation site for calcium/calmodulin-dependent protein kinase II in the NR2B subunit of the N-methyl-D-aspartate receptor. *J. Biol. Chem.* 271, 31670–31678. doi: 10.1074/jbc.271.49.31670
- Paoletti, P., Bellone, C., and Zhou, Q. (2013). NMDA receptor subunit diversity: impact on receptor properties, synaptic plasticity and disease. *Nat. Rev. Neurosci.* 14, 383–400. doi: 10.1038/nrn3504
- Papadia, S., Soriano, F. X., Léveillé, F., Martel, M. A., Dakin, K. A., Hansen, H. H., et al. (2008). Synaptic NMDA receptor activity boosts intrinsic antioxidant defenses. *Nat. Neurosci.* 11, 476–487. doi: 10.1038/nn2071
- Parsons, M. P., and Raymond, L. A. (2014). Extrasynaptic NMDA receptor involvement in central nervous system disorders. *Neuron* 82, 279–293. doi: 10.1016/j.neuron.2014.03.030
- Patneau, D. K., and Mayer, M. L. (1990). Structure-activity relationships for amino acid transmitter candidates acting at N-methyl-D-aspartate and quisqualate receptors. *J. Neurosci.* 10, 2385–2399.
- Perea, G., and Araque, A. (2010). Glia modulates synaptic transmission. *Brain Res. Rev.* 63, 93–102. doi: 10.1016/j.brainresrev.2009.10.005
- Pfrieger, F. W., and Barres, B. A. (1997). Synaptic efficacy enhanced by glial cells *in vitro*. *Science* 277, 1684–1687. doi: 10.1126/science.277.5332.1684
- Robinson, H. P., Sahara, Y., and Kawai, N. (1991). Nonstationary fluctuation analysis and direct resolution of single channel currents at postsynaptic sites. *Biophys. J.* 59, 295–304. doi: 10.1016/s0006-3495(91)82223-8
- Sah, P., Hestrin, S., and Nicoll, R. A. (1989). Tonic activation of NMDA receptors by ambient glutamate enhances excitability of neurons. *Science* 246, 815–818. doi: 10.1126/science.2573153
- Sanz-Clemente, A., Nicoll, R. A., and Roche, K. W. (2013). Diversity in NMDA receptor composition: many regulators, many consequences. *Neuroscientist* 19, 62–75. doi: 10.1177/1073858411435129
- Schwartz, T. L., Sachdeva, S., and Stahl, S. M. (2012). Glutamate neurocircuitry: theoretical underpinnings in schizophrenia. *Front. Pharmacol.* 3:195. doi: 10.3389/fphar.2012.00195
- Sigworth, F. J. (1981). Covariance of nonstationary sodium current fluctuations at the node of Ranvier. *Biophys. J.* 34, 111–133. doi: 10.1016/s0006-3495(81)84840-0
- Steinmetz, C. C., Buard, I., Claudepierre, T., Nägler, K., and Pfrieger, F. W. (2006). Regional variations in the glial influence on synapse development in the mouse CNS. *J. Physiol.* 577, 249–261. doi: 10.1113/jphysiol.2006.117358
- Tang, Y. P., Shimizu, E., Dube, G. R., Rampon, C., Kerchner, G. A., Zhuo, M., et al. (1999). Genetic enhancement of learning and memory in mice. *Nature* 401, 63–69. doi: 10.1038/43432
- Toullec, D., Pianetti, P., Coste, H., Bellevergue, P., Grand-Perret, T., Ajakane, M., et al. (1991). The bisindolylmaleimide GF 109203X is a potent and selective inhibitor of protein kinase C. *J. Biol. Chem.* 266, 15771–15781.
- Traynelis, S. F., and Jaramillo, F. (1998). Getting the most out of noise in the central nervous system. *Trends Neurosci.* 21, 137–145. doi: 10.1016/s0166-2236(98)01238-7
- Ullian, E. M., Sapperstein, S. K., Christopherson, K. S., and Barres, B. A. (2001). Control of synapse number by glia. *Science* 291, 657–661. doi: 10.1126/science.291.5504.657
- Verdoorn, T. A., and Dingledine, R. (1988). Excitatory amino acid receptors expressed in *Xenopus* oocytes: agonist pharmacology. *Mol. Pharmacol.* 34, 298–307.
- von Engelhardt, J., Coserea, I., Pawlak, V., Fuchs, E. C., Köhr, G., Seeburg, P. H., et al. (2007). Excitotoxicity *in vitro* by NR2A- and NR2B-containing NMDA receptors. *Neuropharmacology* 53, 10–17. doi: 10.1016/j.neuropharm.2007.04.015
- Wang, D., Cui, Z., Zeng, Q., Kuang, H., Wang, L. P., Tsien, J. Z., et al. (2009). Genetic enhancement of memory and long-term potentiation but not CA1 long-term depression in NR2B transgenic rats. *PLoS One* 4:e7486. doi: 10.1371/journal.pone.0007486
- Watt, A. J., van Rossum, M. C., MacLeod, K. M., Nelson, S. B., and Turrigiano, G. G. (2000). Activity coregulates quantal AMPA and NMDA currents at neocortical synapses. *Neuron* 26, 659–670. doi: 10.1016/s0896-6273(00)81202-7
- Williams, K. (1993). Ifenprodil discriminates subtypes of the N-methyl-D-aspartate receptor: selectivity and mechanisms at recombinant heteromeric receptors. *Mol. Pharmacol.* 44, 851–859.
- Xiong, Z. G., Raouf, R., Lu, W. Y., Wang, L. Y., Orser, B. A., Dudek, E. M., et al. (1998). Regulation of N-methyl-D-aspartate receptor function by constitutively active protein kinase C. *Mol. Pharmacol.* 54, 1055–1063.
- Xu, J., Xiao, N., and Xia, J. (2010). Thrombospondin 1 accelerates synaptogenesis in hippocampal neurons through neuropilin 1. *Nat. Neurosci.* 13, 22–24. doi: 10.1038/nn.2459
- Yang, K., Jackson, M. F., and MacDonald, J. F. (2014). Recent progress in understanding subtype specific regulation of NMDA receptors by G Protein Coupled Receptors (GPCRs). *Int. J. Mol. Sci.* 15, 3003–3024. doi: 10.3390/ijms15023003
- Zheng, X., Zhang, L., Wang, A. P., Bennett, M. V., and Zukin, R. S. (1999). Protein kinase C potentiation of N-methyl-D-aspartate receptor activity is not mediated by phosphorylation of N-methyl-D-aspartate receptor subunits. *Proc. Natl. Acad. Sci. U S A* 96, 15262–15267. doi: 10.1073/pnas.96.26.15262
- Zito, K., Scheuss, V., Knott, G., Hill, T., and Svoboda, K. (2009). Rapid functional maturation of nascent dendritic spines. *Neuron* 61, 247–258. doi: 10.1016/j.neuron.2008.10.054

Conflict of Interest Statement: The authors declare that the research was conducted in the absence of any commercial or financial relationships that could be construed as a potential conflict of interest.

Copyright © 2015 Hahn, Wang and Margeta. This is an open-access article distributed under the terms of the Creative Commons Attribution License (CC BY). The use, distribution and reproduction in other forums is permitted, provided the original author(s) or licensor are credited and that the original publication in this journal is cited, in accordance with accepted academic practice. No use, distribution or reproduction is permitted which does not comply with these terms.